Eindhoven University of Technology

MASTER

Cathode secondary photoelectron emission by photons a nitrogen discharge

Megens, M.G.M.

Award date:
1994

Link to publication

Disclaimer
This document contains a student thesis (bachelor's or master's), as authored by a student at Eindhoven University of Technology. Student theses are made available in the TU/e repository upon obtaining the required degree. The grade received is not published on the document as presented in the repository. The required complexity or quality of research of student theses may vary by program, and the required minimum study period may vary in duration.

General rights
Copyright and moral rights for the publications made accessible in the public portal are retained by the authors and/or other copyright owners and it is a condition of accessing publications that users recognise and abide by the legal requirements associated with these rights.

- Users may download and print one copy of any publication from the public portal for the purpose of private study or research.
- You may not further distribute the material or use it for any profit-making activity or commercial gain

Take down policy
If you believe that this document breaches copyright please contact us providing details, and we will remove access to the work immediately and investigate your claim.

Download date: 17. Mar. 2025

FACULTEIT ELEKTROTECHNIEK

Vakgroep Hoogspanningstechniek en

Electromagnetic Compatibiliy (EHC)

Cathode secondary photoelectron emission by photons from a nitrogen discharge

door: M.G.M. Megens
EH.94.A.138

De faculteit Elektrotechniek van de Technische Universiteit Eindhoven aanvaardt geen verantwoordelijkheid voor de inhoud van stage- en afstudeerverslagen.

Afstudeerwerk verricht o.l.v.:

J.T. Kennedy, M.Sc.
dr.ir. J.M. Wetzer

april, 1994

TECHNISCHE UNIVERSITEIT EINDHOVEN

Summary

Insulating gases are widely used in electrical power systems and may occasionally suffer electrical breakdown. Such a breakdown results from an excessive number of electrons created from ionization and electron feedback processes. Understanding of these various processes that lead to gaseous breakdown is therefore of great importance. Previously, different numerical simulation models describing the spatio-temporal development of electrons, ions, and excited species have been developed to simulate the initial phases of a gas discharge and can therefore be used for the study of these processes.

In this work a study of the electron feedback process of cathode secondary photoelectron emission by photons from a nitrogen discharge is presented. Cathode secondary photoelectron emission is essential for a Townsend type of breakdown, but also supports the propagation of the cathode streamer in a streamer type of breakdown. Both, numerical simulation and experimental work are combined to gain insight into the parameters associated with photoelectron emission. These parameters are: quenching pressure, lifetime of the excited state, absorption coefficient, cathode quantum efficiency, and excitation coefficient.

It is usually assumed that 3.5 eV photons from the 2^{nd} Positive Group of nitrogen are responsible for secondary photoelectron emission. This excited state has a lifetime of 36 ns. It appears, however, that an excited state having a lifetime of approximately 5 ns is involved. Comparison between the obtained data and literature further suggests that photon energies exceeding 8 eV are created during a nitrogen discharge and play a dominant role in the secondary photoelectron emission process. This implies that the 3.5 eV photons from the 2^{nd} Positive Group are not responsible for secondary photoelectron emission. Absorption appears to play a negligable role. From our experiments, the remaining parameters, quenching pressure, cathode quantum efficiency and excitation coefficient cannot be individually obtained. The quenching pressure however, appears to be much lower than 20 Torr, much lower than the quenching pressure of 60 Torr, representative of the 2^{nd} Positive Group. Instead of the individual parameters, a quantity ω' is defined which depends on the quenching pressure, the cathode quantum efficiency, and the excitation coefficient. ω' can be derived from experiments, and can be used to accurately represent cathode secondary photoelectron emission in discharge models.

Acknowledgement

I would like to thank my coach J.T. Kennedy for his help, patience and time. I must have been a horribly time consuming student. I would like to thank him for all the enlightening discussions we had, both on the subject of the study presented in this report and other topics. I would also like to thank my coach Dr. ir J.M. Wetzer for helping me out all the other times. He is the one who inspired me to go into high-voltage engineering in the first place. Furthermore, I would like to thank all the other people at the High-Voltage and EMC group for the great time.

I would also like to thank my friend Timo van de Put for the same reason he thanks me for in his report: sharing the burden of travelling to Eindhoven by train every day. I thank him and all the other guys for lots of fun.

M.G.M. Megens
Eindhoven, April 1994.

List of symbols

Γ	Cathode electron photoemission quantum efficiency (electrons/photon).
α	Townsend's first ionization coefficient (cm^{-1}).
δ	Excitation coefficient(cm^{-1}).
τ_0	Lifetime of the excited state (s).
μ	Absorption coefficient (cm^{-1}).
Ω	Geometric factor.
$\Delta(x)$	Geometric factor multiplied by $exp(-\mu x)$.
E	Electrical field strength (V/cm).
P	Pressure (Torr).
P_q	Quenching pressure (Torr).
v_e	Electron drift velocity (cm/s).
v_p	Positive ion drift velocity (cm/s).
T_e	Electron transit time of the electrode gap (s).
g	Electrode gap width (cm).
γ_{photon}	Cathode secondary electron emission coefficient.
$\rho_{ex}(t)$	Number density of excited species as a function of time (cm^{-3}).
$\rho_e(t)$	Number density of electrons as a function of time (cm^{-3}).
$\rho_0(t)$	Number density of initial electrons released by the laser (cm^{-3}).
$\rho_{sec}(t)$	Number density of secondary photoelectrons at the cathode as a function of time (cm^{-3}).
$F(r,t)$	Photon flux per unit area per second.
$g(r',x',r)$	Geometric function, defines the normal component of the photon flux at the cathode surface resulting from a source located at (r',x').
$I_{0,e}$	Initial electron current (A).
$I_{prmry,max}$	Maximum primary current (A).
$I_{prmry,max,e}$	Maximum primary electron current (A).
$I_{prmry,max,i}$	Maximum primary ion current (A).
$I_{0sec,e}$	Initial secondary electron current (A).
$I_{sec,max}$	Maximum secondary current (A).
$I_{sec,max,e}$	Maximum secondary electron current (A).
$I_{sec,max,i}$	Maximum secondary ion current (A).
ν	Frequency (Hz).
h	Planck's constant ($h = 6.63 \cdot 10^{-34}$ Js).
e	Elementary charge ($e = 1.6 \cdot 10^{-19}$ C).

Table of contents

Chapter 1

Introduction

My work started out as a study of the discharge inception voltage using both numerical simulations and experiments. In various cases the model did not predict a breakdown, yet the experiments showed a Townsend to streamer type of breakdown. The main problem was the uncertainty in the data regarding cathode secondary photoelectron emission. This data was based on a widely used assumption that secondary photoemission is largely driven by 3.5 eV photons from the 2^{nd} Positive System of nitrogen. Since secondary electron emission is essential for a Townsend type of breakdown, but also supports the propagation of the cathode streamer in a streamer type of breakdown, it was decided that effort should be put into researching cathode secondary photoelectron emission to obtain a set of data more consistent with experiments. In this work a study is presented of secondary photoelectron emission from cathode surfaces using time resolved measurements of avalanche currents, the so called electrical method. The magnitude of the measured secondary electron current maximum in nitrogen has been investigated, while varying pressure, voltage and cathode material. Experimental results are compared to numerical results to gain insight into the parameters associated with photoelectron emission. These parameters are: quenching pressure, absorption coefficient, excitation coefficient, lifetime of the excited state and cathode quantum efficiency.

Chapter 2 describes the fundamental processes that occur in electron avalanches in insulating gases. Also the physical model of an avalanche will be presented here, followed by an example of an avalanche in nitrogen and a short introduction to the simulation model. Chapter 3 describes the experimental setup and experimental procedure used in this work. In chapter 4 a theoretical description of the subject of cathode photoelectron emission by photons from a nitrogen discharge is presented and it is explained how information associated with this process can be extracted from measured current waveforms. The results and conclusions are finally summarized in chapter 5.

Chapter 2

Avalanches in insulating gases

Consider a geometry consisting of two parallel electrodes, between which an insulating gas is located. A DC voltage is applied between the two electrodes, creating a homogeneous electric field. When electrons are released from the surface of the cathode and reach their characteristic drift velocity as determined by the electric field, pressure and gas type, the resulting electron multiplication from collisional ionization is termed an *electron avalanche*. Various processes, like ionization, excitation, attachment etc., occur in such an avalanche and will be described in paragraph 2.1. In paragraph 2.2 the physical model of an avalanche will be presented and paragraph 2.2.2 gives an example of an avalanche in nitrogen.

2.1 Fundamental processes in an avalanche

Immediately after electrons are released from the cathode they are accelerated by the applied electric field, continuously gaining kinetic energy. Electron kinetic energy is lost upon collisions with the heavy background gas species. At the pressures of interest the mean free path between collisions, λ, over which an electron can accelerate, is several orders of magnitude smaller than the distance between the electrodes. The mean energy of an electron can be determined as follows

$$U_e = eE\lambda \tag{2.1}$$

where U_e is the mean energy of the electron, e the charge of an electron, E the electric field and λ the mean free path. The processes of acceleration and collision will balance out very rapidly and result in a constant electron drift velocity in the direction of the field. This drift velocity is superimposed on the random thermal electron velocity, which can usually be described by a Maxwell-Boltzman distribution. Two types of collisions occur: elastic and inelastic. In inelastic collisions a part of the kinetic energy of one particle is used to increase the potential energy of the other particle, while in elastic collisions only kinetic energy is transferred from one particle to the other. This paragraph describes the most important collisional processes occuring in avalanches.

2.1.1 Excitation

In the process of excitation via an inelastic collision, energy of the electron is imparted to the molecular or atomic specie by increasing its potential energy, hence "exciting" the specie.

This means that a valence electron of the atom or molecule will be raised to a higher energy level, where the difference in energy between the previous level and this higher level equals the energy transferred during the collision. Symbolically the reaction may be represented as:

$$e + AB \rightarrow AB^* + e$$

The excitation coefficient, δ, is defined as the number of excitations that occur per unit of lenght.

2.1.2 Relaxation

The excited specie is energetically unstable and therefore the electron raised to the higher energy level will fall back to its ground state after a period of time, τ', the total lifetime of the excited state. A photon may be emitted as the electron makes the quantized transition to lower energy levels. This is termed radiative relaxation. The photon energy will equal the difference between the two energy levels over which the electron falls. Symbolically:

$$AB^{*'} \rightarrow AB^{*''} + h\nu \quad or \quad AB^{*'} \rightarrow AB^{*'} + h\nu$$

Also collisional relaxation or quenching is possible. In this process the excess energy will be transferred to another gas molecule:

$$AB_1^* + AB_2 \rightarrow AB_1^{*'} + AB_2^{*''}$$

in which $^{*'}$ energetic state + $^{*''}$ energetic state = * energetic state. This process of quenching is the dominant relaxation process at higher pressures. The pressure where radiative relaxation starts dominating collisional relaxation depends on the gas and the excited state involved, and is termed the quenching pressure.

2.1.3 Ionization

If the transferred energy during an inelastic collision is greater than the ionization potential, ionization of gas molecules can occur. Effectively ionization can be regarded as the energy needed to place the electron at an infinite distance from the molecule ($\sim$ 14.5 eV for N_2). Ionization does not have to occur by a single inelastic collision, also multiple inelastic collisions can occur before the ionization level is reached. The ionization processes due to electron impact can be expressed by the following reactions:

single ionization	$e + AB \rightarrow AB^+ + 2e$
dissociative ionization	$e + AB \rightarrow A^+ + B + 2e$

The molecule AB may already be excited by previous collisions. Dissociative ionization, as well as single ionization requires a higher electron energy than multiple ionization. The ionization coefficient, α, is defined as the mean number of ionizing collisions of one electron travelling a unit length in the direction of the field.

Photons whith sufficiently high energy can also ionize gas molecules, this process is called gas phase photoionization and will yield a positive ion and an electron, symbolically:

$$h\nu + A \rightarrow A^{+} + e$$

2.1.4 Photoelectron emission

Photoelectron emission is the process whereby photons impinging on a material liberate free electrons. The photon energy should, but does not have to exceed the workfunction of the material. The workfunction is the energy needed to release an electron from a material, and is defined as the difference between the Fermi energy level and vacuum energy level of the material. The number of electrons that will be released per photon is expressed as the quantum efficiency factor, Γ. The quantum efficiency depends strongly on the nature of the material, the material's work function, the presence of any surface contaminates and the energy of the photons striking the cathode surface. In this report the secondary photoelectrons are released by photons emitted by the discharge itself, while the initial electrons are released by a 3.5 eV laser pulse.

2.1.5 Electron attachment

Certain atoms or molecules in their gaseous state can readily acquire a free electron to form a stable negative ion. Gases, wheter atomic or molecular, that have this tendency (electron affinity) are those lacking one or two electrons in their outer shell and are known as electronegative gases. The process of electron attachment may occur in three different ways, described by the following reactions:

dissociative attachment	$e + AB \rightarrow A^{-} + B$
non-dissociative attachment	$e + AB \rightarrow AB^{-}$
three-body attachment	$e + AB_1 + AB_2 \rightarrow AB_1^{-} + AB_2^{*}$

The three-body attachment process is often considered to occur in two stages: First an electron is captured by a gas molecule AB to form an unstable negative ion AB^{-*}:

$$e + AB_1 \rightarrow AB_1^{-*}$$

The energy of an unstable negative ion is higher than that of its ground state. If this unstable negative ion collides with a third body AB_2, it may be converted into a stable negative ion. This process is called *conversion*:

$$AB_1^{-*} + AB_2 \rightarrow AB_1^{-} + AB_2^{*} \quad or \quad AB_1^{-*} + AB_2 \rightarrow AB_1 + AB_2^{-}$$

The energy of a stable negative ion is lower than that of its ground state. The conversion frequency, k_c, is defined as the number of conversions that occur per second per unstable negative ion. The total attachment coefficient, η, is the sum of all attachment processes that produce stable

negative ions, η_{ns}, and all attachment processes that produce unstabele negative ions, η_{nu}.

2.1.6 Electron detachment

The process by which an electron is released by a negative ion is called electron detachment. An unstable negative ion may spontaneously lose its captured electron after a mean lifetime, τ, if it is not collisionally stabilized. This process is called *autodetachment*:

$$AB^{-*} \rightarrow AB + e$$

If the mean time between collisions of the unstable negative ion with neutral gas molecules is much shorter than τ, autodetachment is unlikely to occur. Instead, collisional detachment will occur. Collisional detachment processes, when an unstable negative ion AB^{-*} collides with a gas molecule C, can occur in various ways:

direct detachment	$AB^{-*} + C \rightarrow AB + C + e$
associative detachment	$AB^{-*} + C \rightarrow ABC + e$
dissociative detachment	$AB^{-*} + C \rightarrow A + B + C + e$

Collisional detachment is considered to be the most dominant mechanism under normal gas-discharge conditions. The detachment frequency, k_d, is defined as the mean number of detachments occuring per second per negative ion. This includes detachment from unstable negative ions, k_{ud}, and detachment from stable negative ions, k_{sd}.

Another detachment process is *photodetachment*:

$$h\nu + AB^{-} \rightarrow AB + e$$

This process is unlikely in a practical electrode configuration unless intense light irradiates the gas, or radiation is emitted by the discharge itself with sufficient intensity such as in streamer breakdown.

2.1.7 Ion-ion recombination

The process resulting in the formation of neutral species via collision of a positive and a negative ion is called ion-ion recombination. Ion-ion recombination can occur in two different ways, symbollically expressed in the following reactions:

direct ion-ion recombination	$AB_1^- + AB_2^+ \rightarrow AB_1 + AB_2$
indirect ion ion recombination	$AB_1^- + AB_2^+ \rightarrow (AB_1^- AB_2^+)^*$
	$(AB_1^- AB_2^+)^* + AB_3 \rightarrow AB_1 + AB_2 + AB_3$

The recombination frequency, k_r, is defined as the number of recombinations occuring in a volume per second per positive and negative ion.

2.1.8 Space charge effects

Most of the coefficients mentioned in the preceding paragraphs are in one way or another dependent on the value of the reduced field, E/P, where E is the electric field and P the pressure. In avalanches with low charge densities the field will be constant throughout the interelectrode gap. This constant electric field equivalent to the applied field is called the *Laplacian field*. At higher charge densities the field between the electrons in the head of the avalanche and the positive ions left behind introduces a noticeable distortion in the originally uniform field. The field is enhanced in front of the head of the avalanche with field lines from the anode terminating at the head. Further back in the avalanche, the field between the electrons and the ions left behind reduces the Laplacian field. Still further back the field between the cathode and the positive ions is enhanced again (Fig. 2.1). The coefficients can then no longer be considered constant during the spatio-temporal evolution of the avalanche. In this work only space charge free discharges will be assumed.

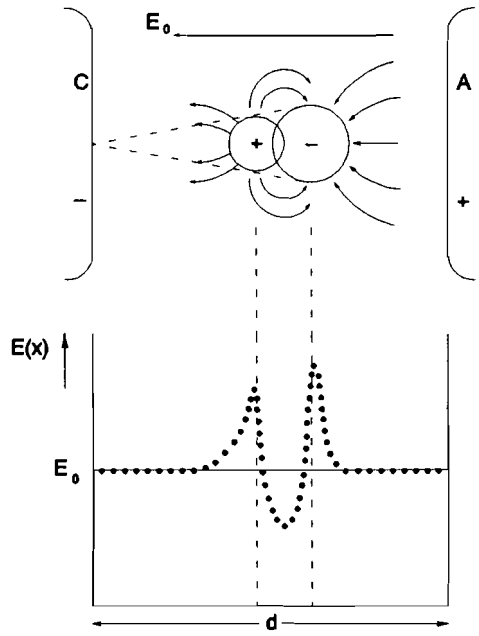

Fig. 2.1 Representation of field distortion in a gap due to the local space charge of an electron avalanche.

2.2 Theoretical description of an avalanche

A theoretical description of an electron avalanche can be obtained by using the *equation of continuity* from fluid dynamics. The continuity equation is a statement of the conservation of mass for fluid flow. Consider a small volume element, see fig. 2.2. Here $\bar{J}$ is the current density and equivalent to:

$$\bar{J} = \rho\bar{v} - D\nabla\rho \tag{2.1}$$

The mass flow through x is $(\rho v)_{in}A$ ("mass"/s) and the mass flow through $x+\Delta x$ is $(\rho v)_{out}A$ ("mass"/s). The mass contained inside the volume element is $\rho A(x+\Delta x-x)$ ("mass"). The change in mass density in time within the volume element is:

$$\frac{\partial\rho}{\partial t} = \lim_{\Delta t\to 0}\left[\frac{\rho(t+\Delta t)A\Delta x - \rho(t)A\Delta x}{\Delta t}\right] \tag{2.2}$$

Since this equals "mass flow out" - "mass flow in" we can rewrite eqn.(2.2):

$$\frac{\partial\rho}{\partial t} = (\bar{J}_{in} - \bar{J}_{out})A \tag{2.3}$$

This can be written as:

$$\frac{\partial\rho}{\partial t} = \lim_{\Delta x\to 0}\left[\frac{A}{A\Delta x}(\bar{J}_{out} - \bar{J}_{in})\right] = \lim_{\Delta x\to 0}\left[\frac{(\bar{J}_{out} - \bar{J}_{in})}{\Delta x}\right] \tag{2.4}$$

This yields:

$$\frac{\partial\rho}{\partial t} = \frac{\partial}{\partial x}\cdot(\rho\bar{v} - D\nabla\rho) \tag{2.5}$$

Eqn.(2.5) is the continuity equation. In general this equation is written as follows:

$$\frac{\partial\rho}{\partial t} + \nabla\cdot(\rho\bar{v} - D\nabla\rho) = S \tag{2.6}$$

The first term in this equation gives the rate, per unit volume, at which mass is accumulating within the volume element. The second term gives the divergence of the *net* outflow of mass from the volume element. The term S is the source or loss of the species in the volume element, for example ionization, attachment, etc..

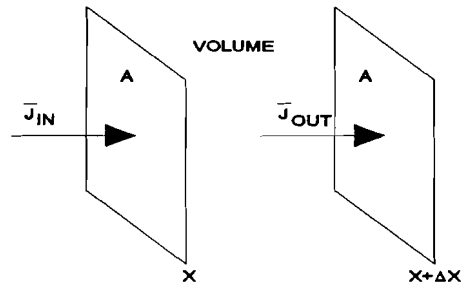

Fig. 2.2 Small volume element.

2.2.1 The physical model

The spatio-temporal variation of the number densities of electrons and ions can described by the following set of continuity equations as defined in the previous section:

$$\frac{\partial \rho_e}{\partial t} + \nabla \cdot (\rho_e \overline{v_e}) = (\alpha - \eta_{nu} - \eta_{ns})\rho_e |v_e| + k_{ud}\rho_{nu} + k_{sd}\rho_{ns} + \nabla \cdot D_e \nabla \rho_e \tag{2.7}$$

$$\frac{\partial \rho_p}{\partial t} - \nabla \cdot (\rho_p \overline{v_p}) = \alpha \rho_e |v_e| - k_r \rho_p (\rho_{nu} + \rho_{ns}) \tag{2.8}$$

$$\frac{\partial \rho_{nu}}{\partial t} + \nabla \cdot (\rho_{nu} \overline{v_{nu}}) = \eta_{nu} \rho_e |v_e| - k_r \rho_p \rho_{nu} - \rho_{nu}(k_{ud} + k_c) \tag{2.9}$$

$$\frac{\partial \rho_{ns}}{\partial t} + \nabla \cdot (\rho_{ns} \overline{v_{ns}}) = \eta_{ns} \rho_e |v_e| + \rho_{nu} k_c - k_r \rho_p \rho_{ns} - \rho_{ns} k_{sd} \tag{2.10}$$

Here $\rho_{e,p,nu,ns}$ are the number densities (cm^{-3}) of electrons, positive ions, unstable negative ions and stable negative ions respectively and $v_{e,p,nu,ns}$ are their respective drift velocities. The coefficients α, η_{nu}, η_{ns}, k_{ud}, k_{sd}, k_r and k_c represent ionization, unstable attachment, stable attachment, unstable detachment frequency, stable detachment frequency, ion-ion recombination frequency and charge exchange (ion conversion) frequency. Electron diffusion is represented by the diffusion tensor D_e. Looking at the source term in eqn.(2.7), the first term on the right represents the production of electrons by ionization, counteracted by unstable and stable attachment, the second and third term represent the production of electrons by unstable and stable detachment respectively.

Secondary photoelectron emission is incorporated as follows. Here, the number density of excited species is described by the following differential equation:

$$\frac{d\rho_{ex}}{dt} = \delta \nu_e \rho_e - \frac{\rho_{ex}}{\tau} \tag{2.11}$$

Here, δ is the excitation coefficient and τ is the mean lifetime of the excited state. Both δ and τ are scaled by $(1+(P/P_q))^{-1}$ where Pq is the quenching pressure, to account for collisional relaxation of the excited species. The number density of secondary photoelectrons generated at the cathode is:

$$\rho_{sec,e}(r,0,t) = \Gamma \frac{F(r,t)}{v_e} \tag{2.12}$$

Here, Γ is the cathode quantum efficiency, and $F(r,t)$ is the photon flux per unit area per second, given by:

$$F(r,t) = \frac{1}{\tau} \int_0^g \int_0^\infty \rho_{ex}(r',x',t) g(r',x',r) r' dr' dx' \tag{2.13}$$

where,

$$g(r',x',r)=\frac{1}{4\pi}\int_0^{2\pi}\frac{x'}{R^3}\exp(-\mu_0\frac{P}{760}R)d\phi \qquad (2.14)$$
$$R=\left(x'^2+r'^2+r^2-2rr'\cos\phi\right)$$

Here, μ_0 is the absorption coefficient, g is the gap width, r' is the radial position of the excited particles (photon source), r is the radial position on the cathode where photoelectron emission occurs, and x' is the axial distance between cathode and photon source. The geometric function $g(r',x',r)$ defines the normal component of the photon flux at the cathode surface resulting from a source located at (r',x'), see fig. 2.3. By considering only the normal flux component, photon reflection off the cathode is approximated.

The set of continuity equations, eqn.(2.7) to (2.10), may not have an analytical solution. Assuming only ionization, attachment, detachment and conversion processes and assuming that the primary electrons are released as a Dirac pulse, the equations can be solved analytically [1]. The solution can be greatly simplified by assuming that the ion drift is negligable if the time scale of interest is short, so that:

$$\nabla\cdot(\rho_i\overline{v}_i)=0 \qquad (2.15)$$

where $i=p,nu,ns$.

Integration of $\rho_{e,p,nu,ns}(x,y,z,t)$ over x, y and z yields the total number of species in the gap at time t $n_{e,p,nu,ns}(t)$:

$$n_{e,p,nu,ns}(t)=\int_x\int_y\int_x\rho_{e,p,nu,ns}(x,y,z,t)\;dxdydz \qquad (2.16)$$

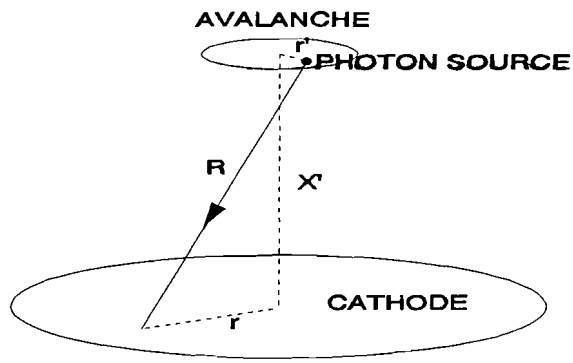

Fig. 2.3 Photon source and cathode configuration used to define g(r',x',r).

2.2.2 Currents caused by moving charges

Charges moving in the interelectrode gap cause an electrical current in the external circuit. The energy necessary to move the charges over a distance dx in a time dt in a direction parallel to the electric field has to be provided by the external circuit:

$$Ui(t)dt = q(t)Edx \tag{2.17}$$

where U is the applied voltage, $i(t)$ is the current caused in the external circuit, $q(t)$ the net charge in the gap and E the electric field experienced by the charge. Hence

$$i_{e,p,nu,ns}(t) = \frac{e\, n_{e,p,nu,ns}(t)\, v_{e,p,nu,ns}\, E}{U} \tag{2.18}$$

where $i_{e,p,nu,ns}(t)$ is the current caused by electrons, positive ions, unstable negative ions and stable negative ions respectively, e is the elementary charge and $n_{e,p,nu,ns}(t)$ and $v_{e,p,nu,ns}$ are the number and axial drift velocity of the respective charged species. The total current caused by the motion of the different species is:

$$i(t) = \sum_{e,p,nu,ns} \left[\frac{eAE}{U} \int_0^g \left[\rho_{e,p,nu,ns}(x,t)\, v_{e,p,nu,ns} + D_{e,p,nu,ns} \frac{\partial \rho_{e,p,nu,ns}(x,t)}{\partial x} \right] dx \right] \tag{2.19}$$

where A is the discharge area and $\rho_{e,p,nu,ns}$ are the respective number densities of the various charged species. The first term in the integrand is the species drift contribution to the current where the summation is over all charged species. The second term is the contribution from the diffusion of the various charged species. By measuring the current, the development of an avalanche can be traced after its initiation. As only electron diffusion is important in this study the second term becomes:

$$D_e \frac{\partial \rho_e(x,t)}{\partial x} \tag{2.20}$$

2.2.3 An example: Nitrogen

In this paragraph an example of an avalanche in nitrogen will be presented. It will be assumed that ions do not drift during the time electrons are present in the gap and radial and axial diffusion will be neglected. Also any secondary effects will be neglected for now. The continuity equations for nitrogen—which is a non-attaching gas—are:

$$\frac{\partial \rho_e(x,t)}{\partial t} + \nabla \cdot (\rho_e v_e) = \alpha \rho_e(x,t) v_e \tag{2.21}$$

$$\frac{\partial \rho_p(x,t)}{\partial t} = \alpha \rho_e(x,t) v_e \tag{2.22}$$

For a space charge free discharge eqn.(2.21) can be rewritten in the hydrodynamic form [1]:

$$\frac{D\rho_e(x,t)}{Dt} = \alpha \rho_e(x,t) v_e \tag{2.23}$$

The electron number densitie for $t \leq T_e$ is calculated by integration of eqn.(2.23). The electron number density is:

$$\rho_e(x,t) = \rho_0 \exp(\alpha v_e t) \tag{2.24}$$

Assuming that the initial electrons are released instantaneously as a Dirac pulse, and since diffusion is neglected here, the initial pulse of electrons will move through the gap at velocity v_e. Assuming no ion drift, the electron and ion number densities for $t \leq T_e$ become [1]:

$$\rho_e(x,t) = n_0 \delta(x - v_e t) \exp(\alpha v_e t) \tag{2.25}$$

$$\rho_p(x,t) = \alpha n_0 \exp(\alpha x) \tag{2.26}$$

where $0 \leq x \leq v_e t$ in eqn.(2.26). The total number of electrons and positive ions can now be calculated [1]:

$$n_e(t) = \int_0^g n_0 \delta(x - v_e t) \exp(\alpha v_e t)\, dx = n_o \exp(\alpha v_e t) \tag{2.27}$$

$$n_p(t) = \int_0^{v_e t} \alpha n_0 \exp(\alpha x) dx = n_0 [\exp(\alpha v_e t) - 1] \tag{2.28}$$

At $t = T_e$ the electrons reach the anode and leave the gap. The formation of ions stops and the positive ions now begin their drift motion toward the cathode with velocity v_p. The number of positive ions can now be calculated for $t > T_e$ [1]:

$$n_p(t) = n_0 \left[\exp\left(\alpha v_e \frac{g + v_p T_e}{v_e + v_p} \right) - \exp\left(\alpha \frac{v_e v_p}{v_e + v_p} t \right) \right] \tag{2.29}$$

The currents caused by the moving charges are:

$$i_e(t) = \frac{e\, n_e(t) v_e}{g} \tag{2.30}$$

$$i_p(t) = \frac{e\, n_p(t) v_p}{g} \tag{2.31}$$

In nitrogen the respective electron and ion drift velocities are:

$$v_e = \mu_e E = \frac{2.9 \times 10^5}{P} E \tag{2.32}$$

$$v_p = \mu_p E = \frac{2 \times 10^3}{P} E \tag{2.33}$$

The electron drift velocity is much greater than the ion drift velocity, so eqn.(2.29) can be approximated by:

$$n_p(t) = n_0[\exp(\alpha g) - \exp(\alpha v_p t)] \tag{2.34}$$

For $t \leq T_e$ the electron current can be represented by:

$$i_e(t) = \frac{e v_e n_0}{g} \exp(\alpha v_e t) = i_o \exp(\alpha v_e t) \tag{2.35}$$

and the positive ion current can be represented by:

$$i_p(t) = \frac{e v_p n_0}{g}[\exp(\alpha v_e t) - 1] = \frac{e v_e n_0}{g}\frac{v_p}{v_e}[\exp(\alpha v_e t) - 1] = \frac{v_p}{v_e} i_0[\exp(\alpha v_e t) - 1] \tag{2.36}$$

For $t > T_e$ all electrons have left the gap and the electron current current becomes zero. The remaining positive ion current can be represented by:

$$i_p(t) = \frac{v_p}{v_e} i_0[\exp(\alpha g) - \exp(\alpha v_p t)] \tag{2.37}$$

By measuring these currents the development of the avalanche can be traced after its initiation. In the next chapter the experimental procedure of avalanche initiation and current measurement will be explained.

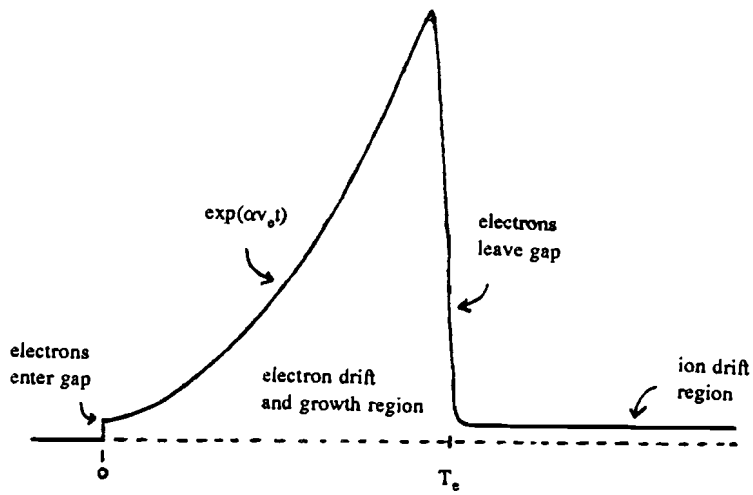

Fig. 2.4 Current waveform of an avalanche in nitrogen.

2.3 Numerical model

The numerical simulation model used in this work has been developed here at the Eindhoven University of Technology [7]. The model solves the set of continuity equations describing the spatio-temporal development of electrons, ions and excited species as presented in paragraph 2.2.1. The continuity equations are solved on a uniform spatial mesh using the flux corrected transport technique (FCT). This algorithm handles steep gradients with minimal numerical diffusion while maintaining numerical stability. Both, a 1 dimensional model and a 2 dimensional model exist. The one dimensional model calculates only axial density distributions and takes axial diffusion into account, where the 2 dimensional model also calculates radial density distributions and takes radial diffusion into account, while assuming cylindrical symmetry. In both models, parameters like pressure, applied voltage, gap width, temperature, number of initial electrons, quantum efficiency, absorption coefficient, quenching pressure, lifetime of excited species and excitation coefficient can easily be set to their appropriate values. As output both models generate the current as a function of time, and number density distributions of electrons and ions as a function of axial and radial position at predefined points in time.

3 Experimental procedure

The experimental procedure used for the avalanche current measurements is the time resolved swarm method—also called electrical method or pulsed Townsend discharge method. This technique is based upon detection of the time dependent current due to electrons and ions drifting across a parallel-plate gap under the influence of the applied uniform electric field. In our experimental setup a short UV laser pulse releases the initial "seed" electrons that initiate the avalanche. The current waveforms obtained give information on the processes occuring and may yield quantitative values for the parameters which describe these processes.

3.1 Experimental setup

A schematic diagram of the experimental setup is shown in fig. 3.1. A subdivided cathode is used for enhanced high frequency response [2]. The aluminum anode is of the Bruce-profile type with an overall diameter of 17 cm. The total diameter of the cathode is 30 cm. The inner measuring disk has a diameter of 4 cm. The annular gap between the two parts is 0.1 mm at the cathode surface. The grounded outer ring is made of aluminum. The avalanche is initiated by a transversely excited atmospheric (TEA) N_2-laser pulse (3.5 eV/photon; 0.6 ns full width at one half maximum; 0.25 mJ/pulse). The light pulse of the laser strikes the cathode through a hole of 1.5 mm diameter in the center of the anode and is focused at the center of the measuring disk. The laser photon energy limits the choice of the cathode material to materials with a work function smaller than or equal to 3.5 eV. The area of the laser spot on the cathode can be changed by changing lens positions, but is kept constant at 0.5 cm^2 in this work. The anode is connected to the DC source by a damping resistor R_d, that protects the voltage source in case of a breakdown of the gap. In addition R_d must be large ($>1M\Omega$) so that nearly all the current travels through the coupling capacitor comprised of the anode and grounded cathode electrodes.

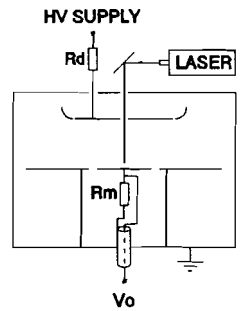

Fig. 3.1 Diagram of experimental setup for the time resolved swarm method.

The moving charges in the gap cause a current in the external circuit comprised of the coupling capacitor, which produces a voltage Vo across the measuring resistor R_m.

The current waveforms are recorded on a Tektronix 7912 AD digitizer.The gap distance can be changed, but is kept constant at 1 cm in this work. The electrodes are placed in a stainless-steel pressure vessel which can be evacuated to 50 μTorr and filled to an absolute pressure of $5.3 \cdot 10^3$ (7 bar). Prior to filling the vessel with the gas to be studied, the chamber is evacuated to 50 μTorr. The pressure and temperature inside the vessel can be measured. The vessel is provided with a long rubber glove which allows the opportunity to operate inside the vessel without opening it. This is only possible when the inside pressure nearly equals the ambient pressure. For higher or lower pressures the holes upon which the glove is fastened can be closed with a cover, the pressure at both sides of the glove is then kept equal by means of a bypass.

Measurements are done, using aluminum (alloy type 6351; 1% Si, 0.6% Mg, 1% Mn) and pure copper and nickel measuring electrodes. Also copper and nickel electrodes with an aluminum insert located at the center, to enhance the number of initial electrons, are used. This is needed as the work functions of these two metals, 4.8 eV for Cu and 5 eV for Ni, are well above the N_2 laser's dominant photon energy, and therefore will release a relatively small number of initial electrons. The diameter of the Al insert is varied from 0.5 to 25 mm. In all measurements, the applied potential is lower than that required for breakdown as determined from the Paschen curve, but high enough to obtain significant secondary electron current.

3.1.1 Measured current and the Ramo-Shockley effect

The subdivided cathode enhances the high frequency response of the measuring setup considerably, however, the radius R of the measuring disk limits the gap width g to a maximum [1,2]. If g becomes too large, the moving charge carriers will also induce a current in the ground connection of the surrounding cathode ring, which reduces the current through R_m. In other words, the current through the measuring resistor R_m depends on R and g and on the position of the charge carriers in the gap. A general formula for the current in the lead to the measuring electrode in a configuration of several electrodes is given by Shockley and Ramo [3,4]:

$$i(t) = \frac{e\,n(t)}{U_{RS}} (\bar{v} \cdot \bar{E}_{RS}) \tag{3.1}$$

Here $i(t)$ is the current in the lead to the measuring electrode caused by a point charge q which moves with velocity v. E_{RS} is the *Ramo-Shockley field* created by a hypothetical voltage U_{RS} applied to the measuring electrode while all other electrodes are grounded.Due to the dot product of the velocity and the Ramo-Shockley field, only the velocity component of the moving charge in the direction of the Ramo-Shockley field results in the measuring disk "seeing" the moving charge. Fig. 3.2 shows the Ramo-Shockley field for the experimental setup. The direction of the velocity vector is of course determined by the real electric field—Laplacian field and space charge

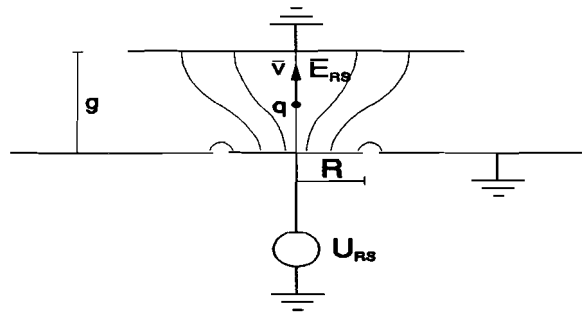

Fig. 3.2 Hypothetical field used in eqn.(3.1) to determine the current i(t).

field. In an earlier study the optimum ratio of disk radius R and gap width g was determined as [2]:

$$\frac{R}{g} \geq 2 \tag{3.2}$$

Hence, in the experimental setup with a measuring disk radius of 2 cm, the gap width is limited to a maximum of 1 cm.

Chapter 4

Cathode photoelectron emission by photons from a gaseous discharge

As an avalanche progresses towards the anode, gas molecules are continuously being excited by collisions with electrons from the avalanche. During the relaxation of the excited species photons may be emitted with sufficient energy to overcome the workfunction of the cathode material, releasing photoelectrons. This process is termed *secondary photoelectron emission.* By means of secondary photoelectron emission a positive feedback of electrons into the gap continuously occurs. To be able to represent secondary photoelectron emission correctly in the simulation model, an accurate mathematical description of the process is needed. To find the right parameters for the mathematical description, information has to be extracted from the measured current waveforms (Fig 4.1).

4.1 Theory

The photons required for cathode secondary photoelectron emission are emitted by particles which were excited by collisions with electrons from the avalanche. The excited state often has a mean lifetime, τ, after which a photon may be emitted. The differential equation describing the change in the number density of the excited species is:

$$\frac{d\rho_{ex}(t)}{dt} = \delta v_e \rho_0 \exp(\alpha v_e t) - \frac{\rho_{ex}(t)}{\tau} \tag{4.1}$$

where δ is the excitation coefficient, v_e the electron drift velocity, ρ_0 the number density of initial electrons, and α the ionization coefficient.

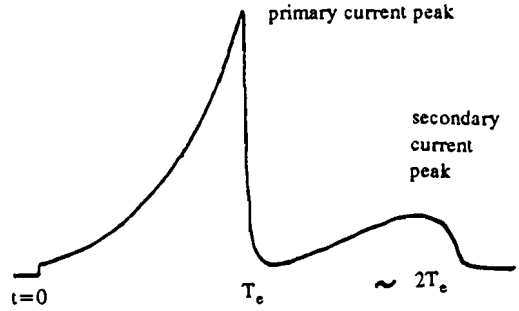

Fig. 4.1 Example of a current waveform with secondary photoelectron emission.

The change in number density of secondary photoelectrons can be represented by:

$$\frac{d\rho_{sec}(t)}{dt} = \Gamma\Delta(x)\frac{\rho_{ex}(t)}{\tau} \tag{4.2}$$

where Γ is the quantum efficiency. The value $\Delta(x)$ equals $\Omega exp(-\mu x)$, where Ω represents a geometric factor and μ is the absorption coefficient. The absorption coefficient has a strong pressure dependence and can be represented by:

$$\mu = \mu_{P_0}\frac{P}{P_0} \tag{4.3}$$

where μ_{P0} is the absorption coefficient at a pressure of P_0.

The solution of eqn.(4.1) yields:

$$\rho_{ex}(t) = \frac{\delta\nu_e\rho_0}{\alpha\nu_e + \frac{1}{\tau}}\left[\exp(\alpha\nu_e t) - \exp\left[-\frac{t}{\tau}\right]\right] \tag{4.4}$$

Approximating that the majority of the excited species are generated just prior to the exit of the primary electron swarm, the integration limits for eqn.(4.2) become T_e to T_e-$(\alpha\nu_e)^{-1}$. This also localizes the $\Delta(x)$ value to $\Delta(g)$. Substitution of eqn.(4.4) into eqn.(4.2) and integrating yields:

$$\rho_{sec}(T_e) = \frac{\Gamma\delta\rho_0\Delta(g)}{\alpha(\tau\alpha\nu_e+1)}\left[\exp(\alpha\nu_e T_e) - \exp\left[\alpha\nu_e\left[T_e - \frac{1}{\alpha\nu_e}\right]\right]\right] \tag{4.5}$$

The exponential relation in eqn.(4.5) is simply $0.63*exp(\alpha\nu_e T_e)$. From measured data it is observed that τ is small, much smaller than $(\alpha\nu_e)^{-1}$, thus making the term $(\tau\alpha\nu_e+1)$ in eqn.(4.5) approximately equal to 1. Finally the number density of electrons, ρ_e for $T_e<t<2T_e$ becomes:

$$\rho_e(T_e < t < 2T_e) = \frac{\Gamma\delta\Delta(g)}{1.6\alpha}\rho_0\exp(\alpha\nu_e T_e)\left[\exp(\alpha\nu_e(t-T_e))\right] \tag{4.6}$$

For $t=2T_e$, ρ_e becomes:

$$\rho_e(2T_e) = \frac{\Gamma\delta\Delta(g)}{1.6\alpha}\rho_0\exp(\alpha\nu_e T_e)\exp(\alpha\nu_e T_e) \tag{4.7}$$

Rewriting this expression yields:

$$\frac{\rho_e(2T_e)}{\exp(\alpha\nu_e T_e)} = \frac{\Gamma\delta\Delta(g)}{1.6\alpha}\rho_0\exp(\alpha\nu_e T_e) \tag{4.8}$$

which can be written as:

$$\rho_{0,\mathrm{sec}} = \frac{\Gamma\delta\Delta(g)}{1.6\alpha}\rho_{prmry,\max} \tag{4.9}$$

where $\rho_{0,sec}$ is the number density of the initial secondary electrons and $\rho_{prmry,max}$ is the maximum number density of the primary electrons.

The secondary photoelectron emission coefficient γ_{photon} can now be defined as follows:

$$\gamma_{photon} = \frac{\rho_{0,sec}}{\rho_{prmry,max}} = \frac{I_{0,sec,e}}{I_{prmry,max,e}} = \frac{\Gamma\delta\Delta(g)}{1.6\alpha} \tag{4.10}$$

where $I_{0,sec,e}$ is the initial secondary electron current, and $I_{prmry,max,e}$ is the maximum primary electron current. The secondary photoelectron emission coefficient is dependent on the cathode material via the quantum efficiency, Γ. The gas-dependent excitation coefficient, δ, is a function of the reduced field, E/P, and pressure, P:

$$\delta\left[\frac{E}{P},P\right] = \delta_0\left[\frac{E}{P}\right]\left[\frac{1}{1+\frac{P}{P_q}}\right] \tag{4.11}$$

where P_q is the quenching pressure. This means that γ_{photon} is dependent on the quantum efficiency Γ, the absorption coefficient μ_0, the excitation coefficient δ_0 and quenching pressure P_q in the following way:

$$\gamma_{photon}\left(\frac{E}{P},P\right) = \frac{\Gamma\Omega\exp\left[-\mu_{P_0}\frac{P}{P_0}g\right]}{1.6\alpha}\delta_0\left(\frac{E}{P}\right)\left[\frac{1}{1+\frac{P}{P_q}}\right] \tag{4.12}$$

Of course γ_{photon} is also dependent on the mean lifetime of the excited state τ, see eqn.(4.5). This can be expected. If τ is small, the excited particles would relax almost imediately after excitation. Since the majority of the excited species is assumed to be generated just prior to the exit of the primary electron swarm, the majority of secondary electrons will now be released almost at the same time. This will result in a secondary avalanche current with a relatively well defined peak. A larger τ would result in secondary electrons being released over a longer period of time after the exit of the primary electron swarm. The result will be that the secondary current peak will be lower and more spread in time. The time constant is also dependent on the quenching pressure:

$$\tau = \left[\frac{\tau_0}{1+\frac{P}{P_q}}\right] \tag{4.13}$$

Since τ is small, much smaller than $(\alpha v_e)^{-1}$, it is expected not to influence γ_{photon}.

4.2 Far UV photons

Optical research done by Legler [5] indicates that 3.5 eV photons from the 2nd Positive System represent the strongest emission band in a nitrogen discharge. It has often been assumed that photons from this system are also responsible for secondary photoelectron emission [10]. Regarding our measurements, information about the time constant has been obtained from comparisons between measured and simulated waveforms (fig. 4.2). In this figure

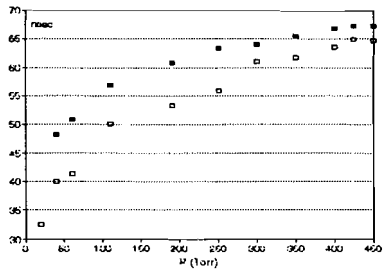

Fig. 4.2 Time elapsed between $I_{sec,max}$ and $I_{prmry,max}$ as a function of pressure; measured (light labels) and simulated (dark labels).

the time elapsed between the primary current peak and the secondary current peak, for both measured and simulated waveforms in N_2 has been presented. For the simulations the excitation coefficient for $C^3\Pi_u$ is used, with τ_0, μ_0 and P_q set to 36 nsec, 0 cm^{-1} and 60 Torr respectively, representative of the 2nd Positive System of N_2. A quantum efficiency of 10^{-4} has been used. It can be seen that the difference between the measured and simulated times decreases with increasing pressure. This is probably due to quenching, since at high pressures the difference in the time constants becomes less important, according to eqn.(4.13). Since in all cases the measured values are less than the simulated ones this suggests that an excited state having a smaller time constant is required.

Upon comparison of laser power output and number of initial electrons released, a quantum efficiency value of roughly 10^{-7} for the aluminum cathode was determined (the pure Cu and Ni cathodes both have an estimated quantum efficiency value of approximately 10^{-9} for 3.5 eV photons). On the other hand a quantum efficiency of 10^{-4} is required to simulate the measured current waveform with an Al cathode if only 3.5 eV (2^{nd} Positive System) photons are assumed. This indicates that photons with energy higher than 3.5 eV are involved, see appendix A. A study using Ni-Al electrodes shows that photoelectron emission is equally likely to occur from the Ni surface as from the Al surface (see paragraph 4.3.4 for more details). Because of the high work function of Ni, photons with energy in excess of 5 eV resulting from excited levels possessing short lifetimes are required. From the above conclusions it can be suggested that 3.5 eV photons do not adequately respresent the observed cathode secondary photoelectron emission.

4.3 Extracting information from experimental current waveforms

Since it is believed that photons from the 2^{nd} Positive System are not responsible for cathode secondary electron emission, information about coefficients representative of the experimental data must be obtained. By measuring current waveforms and using the theory of paragraph 4.1, information may be obtained regarding these coefficients and the photon energy.

4.3.1 The secondary photoelectron emission coefficient: γ_{photon}

According to eqn.(4.10) the cathode secondary photoelectron emission coefficient γ_{photon} is defined as:

$$\gamma_{photon} = \frac{I_{0,sec,e}}{I_{prmry,max,e}} \tag{4.14}$$

where $I_{0,sec,e}$ and $I_{prmry,max,e}$ are the initial secondary and maximum primary *electron* currents respectively. Since the measured current waveforms consist of both electron and ion currents, (positive ion current in the case of nitrogen) the ion currents must be removed, so that an accurate $I_{0,sec,e}$ can be determined. The first current maximum can be described by the following equation:

$$I_{max,1} = I_{prmry,max,e} + I_{prmry,max,i} = I_{0,e}\exp(\alpha g) + \frac{v_p}{v_e} I_{0,e}\left[\exp(\alpha g) - 1\right] \tag{4.15}$$

where $I_{0,e}$ is the number of initial electrons released by the laser, v_e and v_p are the electron and ion drift velocities respectively and g is the gap width. Since the gap width, ionization coefficient α and the electron and ion drift velocities are known quantities, $I_{0,e}$ can be determined from eqn.(4.15). Using the obtained value of $I_{0,e}$, $I_{prmry,max,e}$ and $I_{prmry,max,i}$ can be determined. Since the ion drift velocity is much lower than the electron drift velocity we may assume $I_{prmry,max,i}$ constant after the exit of the primary electron swarm. After the second avalanche has been initiated additional positive ions will be formed, so the second current maximum is:

$$I_{sec,max} = I_{sec,max,e} + I_{prmry,max,i} + I_{sec,max,i} \tag{4.16}$$

Rewriting eqn.(4.16) gives:

$$I_{sec,max} = I_{0,sec,e}\exp(\alpha g) + \frac{v_p}{v_e} I_{0,sec,e}\left[\exp(\alpha g) - 1\right] \tag{4.17}$$

This yields for the initial number of secondary electrons:

$$I_{0,sec,e} = \frac{I_{sec,max} - I_{prmry,max,i}}{\exp(\alpha g) + \frac{v_p}{v_e}\exp(\alpha g) - \frac{v_p}{v_e}} \tag{4.18}$$

Because both $I_{0,sec,e}$ and $I_{prmry,max,e}$ can now be calculated, γ_{photon} can be determined. From eqn.(4.12) we know that γ_{photon} is a function of the reduced field and pressure and that it is related to the quenching pressure, in the following way:

$$\gamma_{photon}\left(\frac{E}{P}, P\right) = \gamma_{photon,0}\left(\frac{E}{P}\right)\left[\frac{1}{1 + \frac{P}{P_q}}\right] \tag{4.19}$$

The γ_{photon} values that can be calculated from measured current waveforms are quenched at an unknown pressure. Fig. 4.3 shows $\gamma_{photon,0}$ data as a function of E/P for different electrodes. This data has been obtained by calculating $\gamma_{photon,0}$(E/P) from γ_{photon}(E/P,P) using eqn.(4.19) with a quenching pressure of 60 Torr.

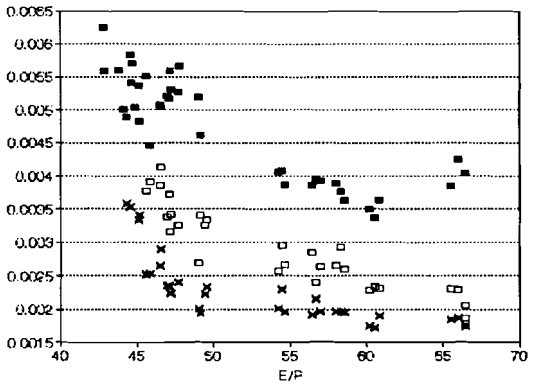

Fig. 4.3 $\gamma_{photon,0}$ as a function of E/P for Al (■), Cu with 0.5 mm Al insert (x) and Cu with 1.0 mm Al insert (□), in N_2 (quenching pressure of 60 Torr used).

Values of $\gamma_{photon,0}$ determined for the Cu control cathode are of the same order of magnitude as the values obtained for the Cu-Al cathodes shown in fig. 4.3, and are lying roughly around 0.002.

Prelimenary $\gamma_{photon,0}$ values for dry air have been obtained from measurements at relatively low pressures to minimize the influence of detachment on the secondary current (E/P values from approximately 57 to 65). Only the Al cathode, and the Cu and Ni cathodes with a 0.5 mm Al insert were used. The $\gamma_{photon,0}$ values obtained with the Al electrode in dry air are approximately 1/3 of the values obtained with the same electrode in N_2. The values obtained with the Cu and Ni electrodes with an Al insert were both approximately 1/3 the values obtained with the Cu cathode with 0.5 mm Al insert in N_2.

4.3.2 Finding the quenching pressure by extrapolation

A possible way of obtaining the quenching pressure from measurements employs the use of eqn.(4.19). Rewriting this equation yields:

$$\frac{1}{\gamma_{photon}(\frac{E}{P},P)} = \frac{1}{\gamma_{photon,0}(\frac{E}{P})}\left[1+\frac{P}{P_q}\right] \qquad (4.20)$$

Plotting $[\gamma_{photon}(E/P,P)]^{-1}$ as a function of pressure while keeping E/P constant results in a straight line. Doing this for various E/P values, an extrapolation to $[\gamma_{photon}(E/P,P)]^{-1}=0$ can be made (see fig. 4.4). From eqn.(4.20) we see that if $[\gamma_{photon}(E/P,P)]^{-1}$ equals 0, P has to equal the quenching pressure, P_q. So, measurements done at constant E/P and varying pressure may yield the quenching pressure through extrapolation. However, the pressure ranges over which E/P could be maintained constant without initiating a breakdown and still seeing secondary photoelectron emission, turned out to be so small that no reasonable extrapolation could be obtained.

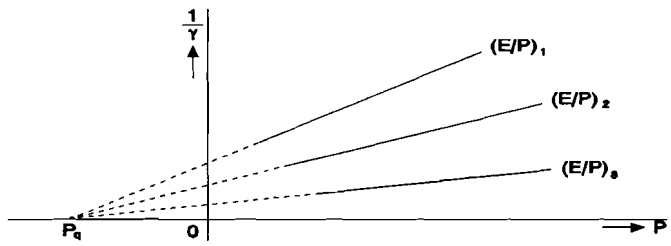

Fig. 4.4 Finding the quenching pressure by extrapolation.

4.3.3 The excitation coefficient: δ

Because of γ_{photon} depending on the measuring environment via the quantum efficiency, Γ, and a geometric factor Ω, it is not a useful parameter that can be used to describe secondary photoelectron emission in general. A much more useful parameter to achieve this goal is the gas dependent excitation coefficient, δ. This coefficient can be calculated from the γ_{photon} data in the following way:

$$\delta(\frac{E}{P},P)=\frac{1.6\alpha}{\Gamma\Delta(g)}\gamma_{photon}(\frac{E}{P},P) \tag{4.21}$$

The quantum efficiency, Γ, depends on the photon energies involved and since these photon energies are unknown, the quantum efficiency is also unknown. This means that only the product of quantum efficiency and excitation coefficient, $\Gamma\cdot\delta(E/P,P)$, can be determined:

$$\Gamma\delta(\frac{E}{P},P)=\frac{1.6\alpha}{\Delta(g)}\gamma_{photon}(\frac{E}{P},P) \tag{4.22}$$

Dequenching eqn.(4.22) using any quenching pressure value P_q', yields $\Gamma\cdot\delta_0(E/P)$:

$$\Gamma\delta_0(\frac{E}{P})=\frac{1.6\alpha}{\Delta(g)}\gamma_{photon}(\frac{E}{P},P)\left[1+\frac{P}{P_q'}\right] \tag{4.23}$$

The result is a gas specific function that only depends on the reduced field, E/P. The pressure reduced excitation coefficient, $\delta_0(E/P)/P$, can be assumed to have the following form:

$$\frac{\delta_0(\frac{E}{P})}{P}=A\exp\left[-\frac{B}{\left[\frac{E}{P}\right]}\right] \tag{4.24}$$

So the pressure reduced product $\Gamma\cdot\delta_0(E/P)/P$ shows the same general form:

$$\frac{\Gamma\delta_0(\frac{E}{P})}{P}=C\exp\left[-\frac{B}{\left[\frac{E}{P}\right]}\right] \tag{4.25}$$

This means that plotting the logarithm of $\Gamma\cdot\delta_0(E/P)/P$ will show a straight line:

$$\ln\left[\frac{\Gamma\delta(\frac{E}{P})}{P}\right]=\ln(C)-\frac{B}{\left[\frac{E}{P}\right]} \tag{4.26}$$

Fitting a straight line through the data points yields the coefficients B and C. A functional relationship $(\Gamma\cdot\delta_0(E/P)/P)^{fit}$ can thus be obtained, and incorporated in the numerical simulation model. Of course, requenching of this functional relationship using P_q' also has to be taken care of in the numerical model in the following way:

$$\Gamma\delta(\frac{E}{P},P)=P\left[\frac{\Gamma\delta_0(\frac{E}{P})}{P}\right]^{fit}\left[\frac{1}{1+\frac{P}{P_q'}}\right] \tag{4.27}$$

where P_q' has to have the same value as used for dequenching in eqn.(4.23).
This data can be used in the numerical simulation model. Varying τ_0 and P_q, and comparing simulations with measurements, can give an idea of the values of these parameters. Regarding the absorption coefficient, data from literature [6] indicates that a value for μ_0 of less than 5 may be expected, but as of present cannot be verified.

Functional relationships of $\Gamma\cdot\delta_0(E/P)/P$ dequenched at 1, 30 and 60 Torr have been obtained and incorporated in the numerical simulation model. Simulations resulted in excessive secondary emission and even breakdown where experiments did not show this. However, the values of $\gamma_{photon}(E/P,P)[exp(\alpha v_e T_e)-1]$ were less than 1 in all cases, which indicates that no breakdown should occur.

A possibility of error is the fact that in eqn.(4.7) it is assumed that the secondary current peak lies approximately at $t\simeq 2T_e$. In fig. 4.9 it can be seen that this is not the case. The time elapsed between the primary maximum and the secondary maximum is approximately $0.8T_e$ in all cases. This means that some error occurs when calculating γ_{photon} and thus yielding wrong values for the excitation coefficient, δ. Also, the simple model assures a simple 1D geometric factor $<g(r',x',r)$. A better geometric factor should be incorporated. As of now, no direct information regarding $\Gamma\cdot\delta_0(E/P)/P$ can be obtained from the experimental current waveforms. But as to be discussed in section 4.2, by comparing simulations with the measured waveforms we were able to extract some information about $\Gamma\delta_0(E/P)/\alpha$. Information regarding the photon energy has been obtained and will be discussed in the next section.

4.3.4 The photon energy

Information regarding the photon energy has been obtained by studying the ratios of secondary current amplitudes for the Cu-Al, Ni-Al and Al electrodes. Since Cu and Ni cathodes with Al inserts are used, the role of these inserts regarding their participation in the release of secondary photoelectrons has to be taken into account. Fig. 4.5 shows results from Kennedy [7] in which the reduced secondary currents are plotted as a function of Al insert area to laser spot area for the Ni electrode. Each label represents a separate E/P value. The solid line is the average initial current ratio, $I_{0,e}(Ni\text{-}Al)/I_{0,e}(100\%\ Al)$. It is observed that the secondary current ratio and initial current ratio show the same trend with regards to the ratio of Al insert area and laser spot area. The meaning of this plot can be explained as follows. From eqn.(4.9), rewritten in electron current form, it can be seen that in reduced form the only terms that play a role are those involving the material dependencies i.e.:

$$\frac{I_{0,sec}\,|_{Al\text{-}Ni}}{I_{0,sec}\,|_{Al}} = \frac{\Gamma_{Al\text{-}Ni}}{\Gamma_{Al}} \frac{I_0\,|_{Al\text{-}Ni}}{I_0\,|_{Al}} \tag{4.28}$$

Because $(I_{0,sec}\,|_{Al\text{-}Ni})/(I_{0,sec}\,|_{Al})$ is identical with $(I_0\,|_{Al\text{-}Ni})/(I_0\,|_{Al})$ it can be stated that $\Gamma_{Al\text{-}Ni}/\Gamma_{Al} \approx 1$ or in other words emission is equally likely to occur from the Ni surface as from the Al surface.

To obtain some idea of the photon energies involved the following procedure was used. From eqn.(2.12) we know that the number density of secondary photoelectrons generated at the cathode is:

$$\rho_{sec}(r,0,t) = \Gamma \frac{F(r,t)}{v_e} \tag{4.29}$$

where the term $F(r,t)$ has previously been defined in section 2.2.1.

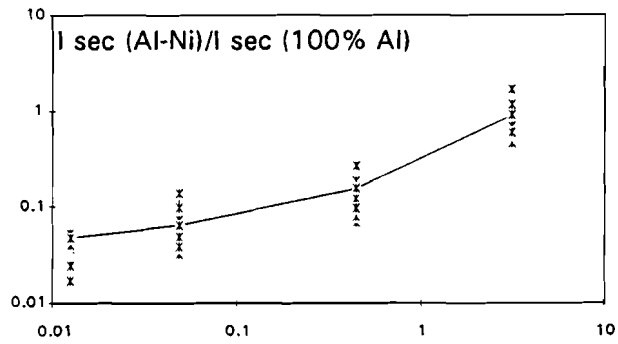

Fig. 4.5 Reduced secondary currents as a function of Al insert area to laser spot area for the Ni electrode.

The initial secondary electron current $I'_{sec,0,e}$ from the Cu-Al or Ni-Al cathode can be proportionally represented by:

$$I'_{sec,0,e} \propto \Gamma_{Al} \int_0^{R_{Al}} F(r,T_e) r dr + \Gamma' \int_{R_{Al}}^{R} F(r,T_e) r dr \tag{4.30}$$

in which Γ' represents either the Cu or the Ni cathode quantum efficiency. Eqn.(4.30) states that the number of secondary electrons is equal to the contribution from the Al insert plus the contribution from the Ni or Cu section. Of course the number density of the excited species $N_{ex}(r',x',T_e)$ in $F(r,T_e)$ is not known in this case, so only the reduced quantum efficiency values, Γ'/Γ_{AL}, can be obtained:

$$\frac{I'_{sec,0,e}}{I^{Al}_{sec,0,e}} \cdot \frac{I^{Al}_{0,e}}{I'_{0,e}} = \frac{\int_0^{R_{Al}} F(r,T_e) r dr}{\int_0^{R} F(r,T_e) r dr} + \frac{\Gamma'}{\Gamma_{Al}} \frac{\int_{R_{Al}}^{R} F(r,T_e) r dr}{\int_0^{R} F(r,T_e) r dr} \tag{4.31}$$

The function $F(r,T_e)$ is adequately represented by a Gaussian function, as has been determined by Kennedy [7], and R is the total radius of the measuring cathode, and R_{Al} is the aluminum insert radius. Fig. 4.6 shows Γ_{Cu}/Γ_{Al} and Γ_{Ni}/Γ_{Al} as a function of pressure for different Al insert areas. Up to 220 Torr the Cu-Al and Ni-Al Γ ratios are approximately 0.8 and 0.6 respectively. Above 220 Torr a linear increase with pressure is observed for both, Γ_{Cu}/Γ_{Al} and Γ_{Ni}/Γ_{Al}. This may be due to the neglection of absorption in the simulations [7].

Quantum efficiency data in the literature (see Appendix A) covers pure metals like Cu and Ni, and not alloys like the Al used for the Al control cathode and the inserts of the Cu and Ni cathodes. This means that only the Γ_{Ni}/Γ_{Cu} ratios can be used for comparison with literature. In fig. 4.6 this ratio is approximately 1.3.

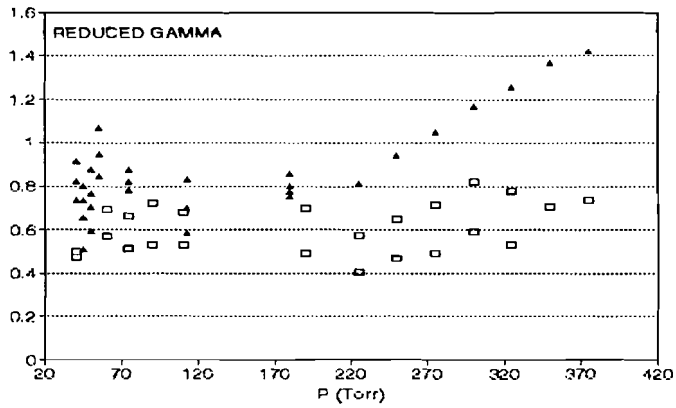

Fig. 4.6 Plot of Γ_{Ni}/Γ_{Al} (▲) and Γ_{Cu}/Γ_{Al} (□) as a function of pressure for different Al inserts.

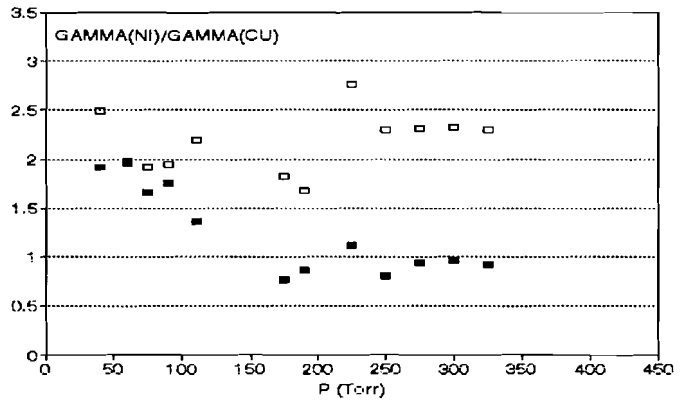

Fig. 4.7 Plot of Γ_{Ni}/Γ_{Cu} for Ni and Cu cathodes with 15 mm Al insert (■) and 25 mm Al insert (□).

Fig. 4.7 shows Γ_{Ni}/Γ_{Cu} as a function of pressure for Ni and Cu cathodes with Al insert diameters of 15 and 25 mm, and here Γ_{Ni}/Γ_{Cu} is approximately 1.5. Comparing this ratio of approximately 1.5 with literature [8,9] (Appendix A, fig. A2 and fig. A3), showed that photon energies in excess of 8 eV are needed to explain the results. So, photon energies in excess of 8 eV but less than 14 eV (the ionization potential of nitrogen) appear to be responsible for cathode secondary photoelectron emission.

The cathode quantum efficiency appears to stay quite constant during a set of measurements, as can be concluded from fig 4.8. Here the current resulting from the release of initial electrons by the laser (I_0) is plotted as a function of pressure. Each label represents a seperate measurement. Only after a breakdown has occured will the number of initial electrons drop, but will thereafter again remain approximately constant.

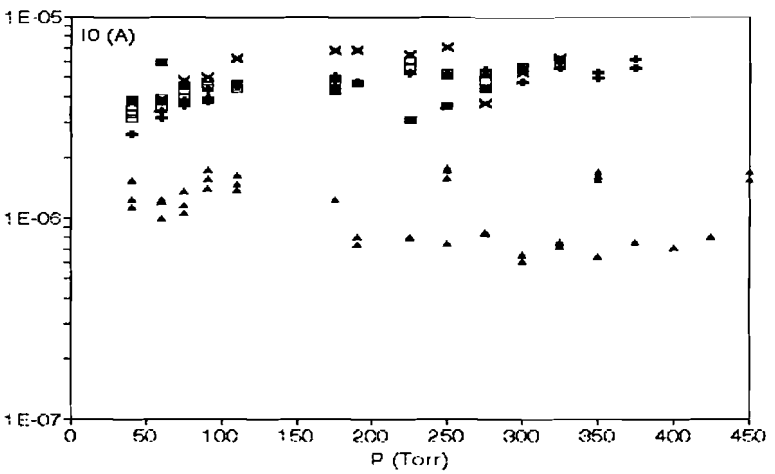

Fig. 4.8 Plot of initial current I_0 as a function of pressure for the Al (▲), and Cu measuring cathode with 0.5 mm (□), 1.0 mm (+), 15.0 mm (X), and 25.0 mm (■) Al insert.

4.4 Combining simulation and experiment to extract physical parameters

Because photon energies in excess of 8 eV are required to explain the results, the energies are much closer to the nitrogen ionization potential of 14 eV than the 3.5 eV photons from the 2nd Positive System. This indicates that the excitation coefficient may have the following form:

$$\delta(\frac{E}{P},P)=\omega\alpha\left[\frac{1}{1+\frac{P}{P_q}}\right] \tag{4.32}$$

in which ω will probably depend on the reduced field, E/P. If an excitation coefficient of this form is incorporated in the numerical simulation model, the resulting current waveforms can be compared with experimentally obtained current waveforms, and the error in the secondary maximum current, ϵI, and the error in the secondary maximum time, ϵT, as a function of P_q, μ_0, τ_0, Γ and ω can be studied. From paragraph 4.4.1 it is known that γ_{photon} depends on these parameters in the following way:

$$\gamma_{photon}(\frac{E}{P},P)=\frac{\Gamma\Omega\exp\left[-\mu_{P_0}\frac{P}{P_0}x\right]}{1.6\alpha\left[\tau_0\alpha\nu_e(1+\frac{P}{P_q})^{-1}+1\right]}\delta_0(\frac{E}{P})\left[1+\frac{P}{P_q}\right]^{-1} \tag{4.33}$$

For large values of P/P_q ratio this equation can be approximated through a binomial expansion by:

$$\gamma_{photon}(\frac{E}{P},P)\approx\frac{\Gamma\Omega\exp(-\mu_0\frac{P}{760})}{1.6\alpha}\delta_0(\frac{E}{P})\left[\frac{P_q}{P}-\tau_0\alpha\nu_e\left[\frac{P_q}{P}\right]^2\right] \tag{4.34}$$

Because the quantum efficiency is not known the following parameter will be defined:

$$\omega'=\Gamma\omega=\frac{\Gamma\delta_0(\frac{E}{P})}{\alpha} \tag{4.35}$$

Rewriting eqn.(4.33) now gives:

$$\gamma_{photon}(\frac{E}{P},P)\approx\omega'\Omega\exp(-\mu_{P_0}\frac{P}{P_0})\left[\frac{P_q}{P}-\tau_0\alpha\nu_e\left[\frac{P_q}{P}\right]^2\right] \tag{4.36}$$

From this equation it can be concluded that ϵI will change linearly with ω' and approximately linear with P_q for large P/P_q, and exponentially with the absorption coefficient μ_0. Almost no dependence on τ_0 is expected for large P/P_q.

The error in time ϵT is a function of τ_0, Pq and also μ_0. It will change linearly with τ_0 and approximatly linear with P_q for high P/P_q ratios. The secondary maximum time depends on absorption because if absorption is high, only photons emitted from the avalanche close to the cathode are able to liberate electrons from the cathode material. The secondary peak will occur earlier in time than if absorption were low. If the avalanche is still close to the cathode, the number density of excited species will be low. This means that relatively few photons will be emitted from the avalanche and so the current maximum will be lower and more spread in time. An increase of absorption is expected to show a proportional decrease in secondary maximum time.

A study of the effects of all these parameters on the secondary maximum current and time showed the expected dependencies. Only for very small τ_0 (less than 1 nsec) a sharp increase in secondary current occured which may be due to numerical instabilities. Unsuccessful attempts have been made to find an analytical function for $\epsilon I + \epsilon T$ with the goal of minimizing it. Because of the complex nonlinear effect of these coupled parameters on the secondary current, many combinations of ω', P_q, τ_0 and μ_0 are possible.

By making educated guesses of the parameters involved, based on comparison between experiment and simulation, a reduction of variables may be obtained. By comparing simulations of secondary photoelectron emission from the 2nd Positive Group with measured current waveforms, it can be concluded that a much smaller time constant is needed to explain the the observed results (see fig. 4.2). Some other important observations can be made from fig. 4.9. The ratio of the time elapsed between the primary maximum and secondary maximum ΔT, and the electron transit time T_e, shows no pressure dependence from 20 to 450 Torr. The secondary maximum time is determined by the time constant τ_0, the quenching pressure P_q, and the amount of absorption, represented by μ_0. This pressure independence indicates that absorption can be neglected and that P/P_q is quite high. If absorption would play a role, the time of the secondary maximum would decrease with increasing pressure. If P/P_q would be low, there would also be a pressure dependence, because of τ being scaled by $(1+(P/P_q))^{-1}$, see fig. 4.10. However, no pressure dependence is observed at all.

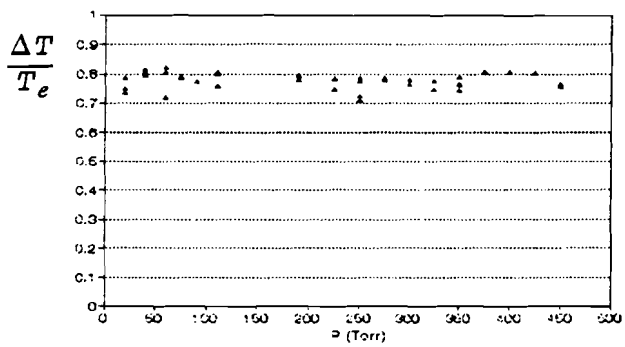

Fig. 4.9 Ratio of the time elapsed between $I_{sec,max}$ and $I_{prmry,max}$ and the electron transit time T_e as a function of pressure in N_2.

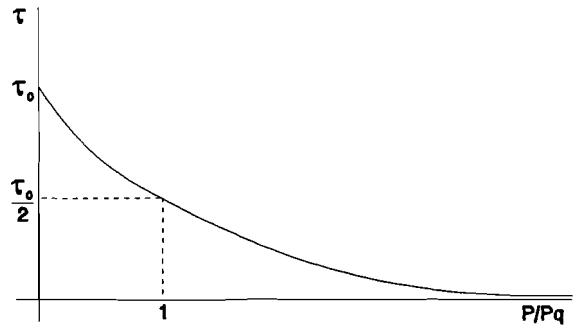

Fig. 4.10 Time constant τ as a function of P/P_q

Preliminary data of the ratio of the time elapsed between the primary maximum and secondary maximum ΔT, and the electron transit time T_e, obtained from measurements in dry air, also shows a pressure independence from 40 to 250 Torr. The value of this ratio is approximately 0.75, just as in nitrogen.

Since τ_0 has a negligable influence on the heigth of the secondary current maximum at high P/P_q ratios, a value for τ_0 can be obtained via simulations by studying ΔT for different pressures as a function of τ_0. An experimentally obtained value of 5 nsec for τ_0 works well with quenching pressures up to 60 Torr. Because $\Delta T/T_e$ is pressure independent from 20 Torr and up, it can be concluded that P_q has to be much lower than 20 Torr.

Using values of 0 and 5 nsec for μ_0 and τ_0 respectively in the numerical simulation model, $\omega'=\Gamma\omega$ can be studied for different quenching pressures as a function of the reduced field E/P. For various values of the reduced field, simulations can be compared to measured current waveforms. The quenching pressure was kept constant at some arbitrary value, and ω' set to some arbitrary value that resulted in a pronounced secondary maximum.

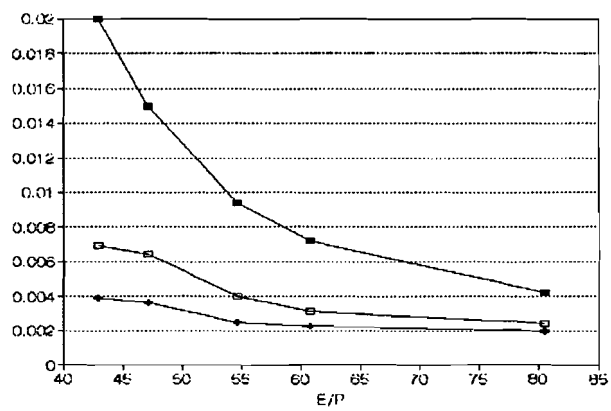

Fig. 4.11 Plot of ω'_{opt} as a function of the reduced field E/P, for quenching pressures of 10 Torr (■), 30 Torr (□) and 60 Torr (+).

Because this secondary maximum current scales proportional with ω', an optimum can be determined for this parameter:

$$\omega'_{opt} = \omega'_{sim} \frac{I_{sec,max,sim}}{I_{sec,max,meas}} \tag{4.37}$$

Here, ω'_{sim} represents the value used in the simulation, and $I_{sec,max,sim}$ and $I_{sec,max,meas}$ are the simulated and measured maximum secondary current respectively. Comparing simulations with experimental current waveforms obtained with the Al electrode, for various E/P values, and using different quenching pressures in the simulations, a plot can be made that shows ω'_{opt} as a function of E/P for various P_q, see fig. 4.11. Implementing a functional relationship of one of the curves in the numerical simulation model, and quenching it at the corresponding P_q represents the process of secondary photoelectron emission quite well. Fig. 4.12 and fig 4.13 show measured and simulated current waveforms. The simulated waveforms were obtained with the calculated values for ω'_{opt} for P_q=10, and μ_0, τ_0 set to 0 and 5 ns respectively.

Since ω'_{opt} is defined as $\Gamma\delta_0/\alpha$ a comparison can be made with Legler's δ_0/α data [5], which has been obtained by dequenching at 60 Torr—the quenching pressure representative of the 2nd Positive System of nitrogen. Both ω'_{opt} at P_q=60 Torr and a scaled version af Legler's data are plotted in fig. 4.14. The descrepancy also supports the idea that photons from the 2nd Positive System are not responsible for photoelectron emission.

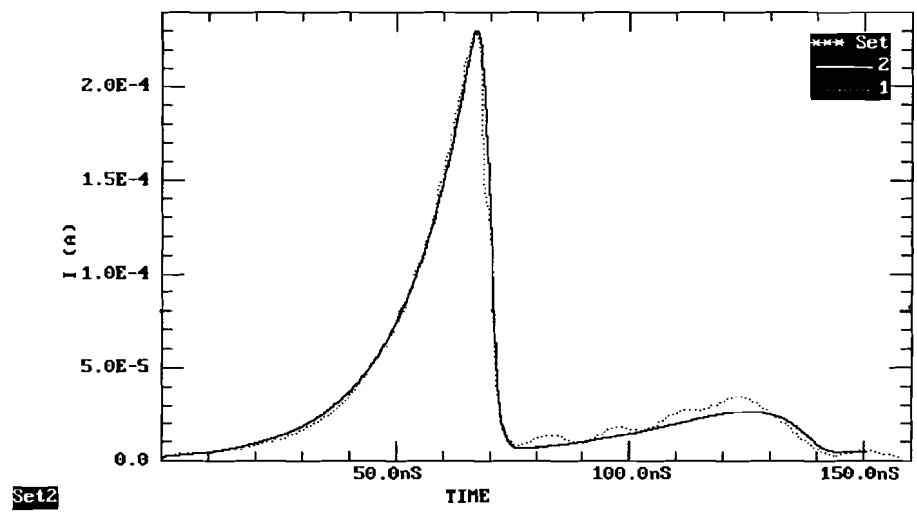

Fig. 4.12 Measured (...) and simulated (—) current waveform at P=250 Torr, and E/P=47.16. P_q=10, μ_0=0, τ_0=5 ns and ω'=1.5E-2 used in simulation.

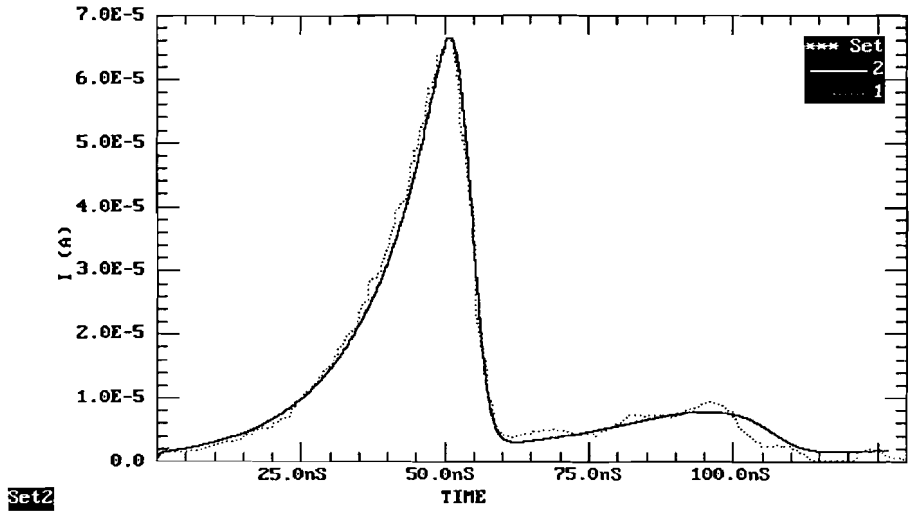

Fig. 4.13 Measured (...) and simulated (—) current waveform at P=60 Torr, and E/P=60.83. P_q=10, μ_0=0, τ_0=5 ns and ω'=7.18E-3 used in simulation.

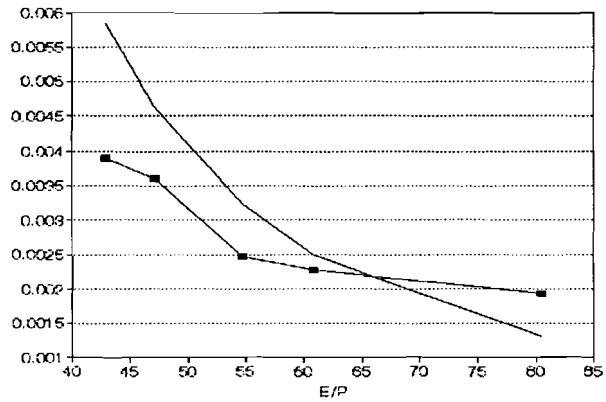

Fig. 4.14 Plot of ω'_{opt} for P_q=60 Torr (dark labels) and scaled data of Legler (single line).

Chapter 5

Conclusions

An experimental study of electron avalanches in nitrogen has been performed with emphasis on secondary photoelectron emission from the cathode surface. Three cathode types; aluminum, nickel, copper, and nickel and copper with aluminum inserts were used in this study, and in all cases secondary electron emission is observed. Comparison between the data obtained in this study and literature suggests that photon energies exceeding 8 eV are created during discharges in nitrogen and play a dominant role in the secondary photoelectron emission process.

Insight into the parameters directly associated with secondary photoelectron emission has been gained. These parameters are: quenching pressure, absorption coefficient, mean lifetime of the excited state, cathode quantum efficiency, and excitation coefficient.

Absorption appears to play a negligable role in the process of secondary photoelectron emission. The time constant of the excited state involved appears to be much smaller than the one representative of the 2^{nd} Positive Group of nitrogen. A value of 5 nsec for τ_0—instead of 36 nsec for the 2^{nd} positve group—seems to represent the involved state quite well. As of now, the remaining parameters, quenching pressure, cathode quantum efficiency and excitation coefficient cannot be obtained individually. The quenching pressure however, appears to be much lower than 20 Torr.

Instead of the individual parameters, a combined representation of the quenching pressure, cathode quantum efficiency and excitation coefficient has been obtained in the form of $\omega' = \Gamma\delta_0/\alpha$ as a function of the reduced field E/P, for various quenching pressures. A functional relationship can be obtained from one of these curves. Implemented in the numerical simulation model, the process of secondary photoelectron emission is accurately represented, although not all the parameters are individually known.

References

[1] Wen, C.
TIME-RESOLVED SWARM STUDIES IN GASES WITH EMPHASIS ON ELECTRON DETACHMENT AND ION CONVERSION
Proefschrift Technische Universiteit Eindhoven
Wibro dissertatie drukkerij, Helmond, 1989

[2] Verhaart, H.F.A.
AVALANCHES IN INSULATING GASES
Proefschrift Technische Universiteit Eindhoven
Wibro dissertatie drukkerij, Helmond, 1982

[3] Shockley, W.
CURRENTS TO CONDUCTORS INDUCES BY A MOVING POINT CHARGE
Journal of Applied Physics, Vol. 9(1938), p. 635-636

[4] Ramo, S.
CURRENTS INDUCED BY ELECTRON MOTION
Proceedings IRE, Vol. 27(1939), p. 584-585

[5] Legler, W
ANREGUNG VON UV-STRAHLUNG IN STICKSTOFF UND WASSERSTOFF DURCH EINEN ELEKTRONENSCHWARM
Zeitschrift für Physik, 173(1963), p. 169-183

[6] Cook, G.R. and P.H. Metzger
PHOTOIONIZATION AND ABSORPTION CROSS SECTIONS OF O_2 AND N_2 IN THE 600- TO 1000-Å REGION
The Journal of Chemical Physics, Vol. 41(1964), No. 2, p. 321-336

[7] Kennedy J.T., M.G.M. Megens and J.M. Wetzer
CATHODE PHOTOELECTRON EMISSION DURING A GAS DISCHARGE IN N_2 AND DRY AIR
IEEE Symposium on electrical insulation, Pittsburgh, June 1994

[8] Schäfer, K.
EIGENSCHAFTEN DER MATERIE IN IHREN AGGREGATZUSTÄNDEN
Berlin: Springer, 1959
Zahlenwerte und Functionen aus Physik, Chemie, Astronomie, Geophysik und ..., Bd. 2

[9] Flügge, S.
ELECTRON EMISSION AND GAS DISCHARGES 1
Berlin: Springer, 1956
Handbuch der Physik, Bd. 21

[10] Tagashira, H. and K. Yoshida
COMPUTER SIMULATION OF A NITROGEN DISCHARGE AT HIGH OVERVOLTAGES
J. Phys. D: Appl. Phys., Vol. 9(1976), p. 491-505

Appendix A

Fig. A1 is a diagram of the electronic and vibrational energy levels of the nitrogen molecule. The most important of the allowed transitions, including the 2nd Positive Group, are indicated by the arrows. Fig. A2 shows quantum efficiency data for various metals as a function of wavelength [8]. The quantum efficiency increases with decreasing wavelength, and thus increasing energy. The quantum efficiency of the Al cathode is estimated to be approximately 10^{-7} for 3.5 eV photons. The Al used in our measurements is an alloy, and not accurately represented by this quantum efficiency data. In simulations, where the excitation coefficient of $C^3\Pi_u$ is used, together with values of τ_0, μ_0 and P_q representative of the 2nd Positive Group, a quantum efficiency of 10^{-4} is needed to simulate current waveforms with a secondary current maximum of the same magnitude as that measured. This indicates that photons with energy >3.5 eV are required to explain the results.

From measurements of the initial electron number, the pure Cu and Ni cathodes both have an estimated quantum efficiency value of approximately 10^{-9}. This approximately agrees with the quantum efficiency data in fig. A2 for 3.5 eV photons. On the other hand, measurements of the secondary photoelectron emission indicated that $\Gamma_{Ni/Cu}$ is approximately equal to Γ_{Al} (see figures 4.5 and 4.6). Therefore, from fig. A2 it can be concluded that the photon energies involved must be at least >5 eV.

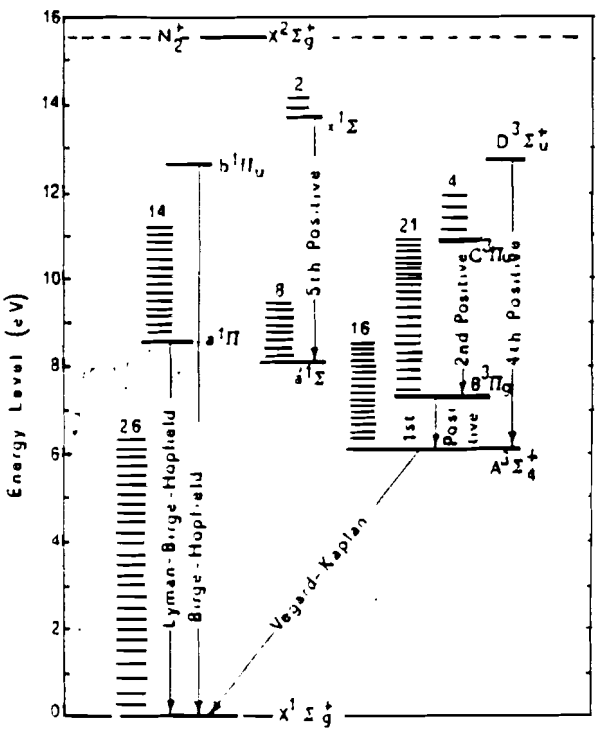

Fig. A1 Diagram of energy levels of the nitrogen molecule.

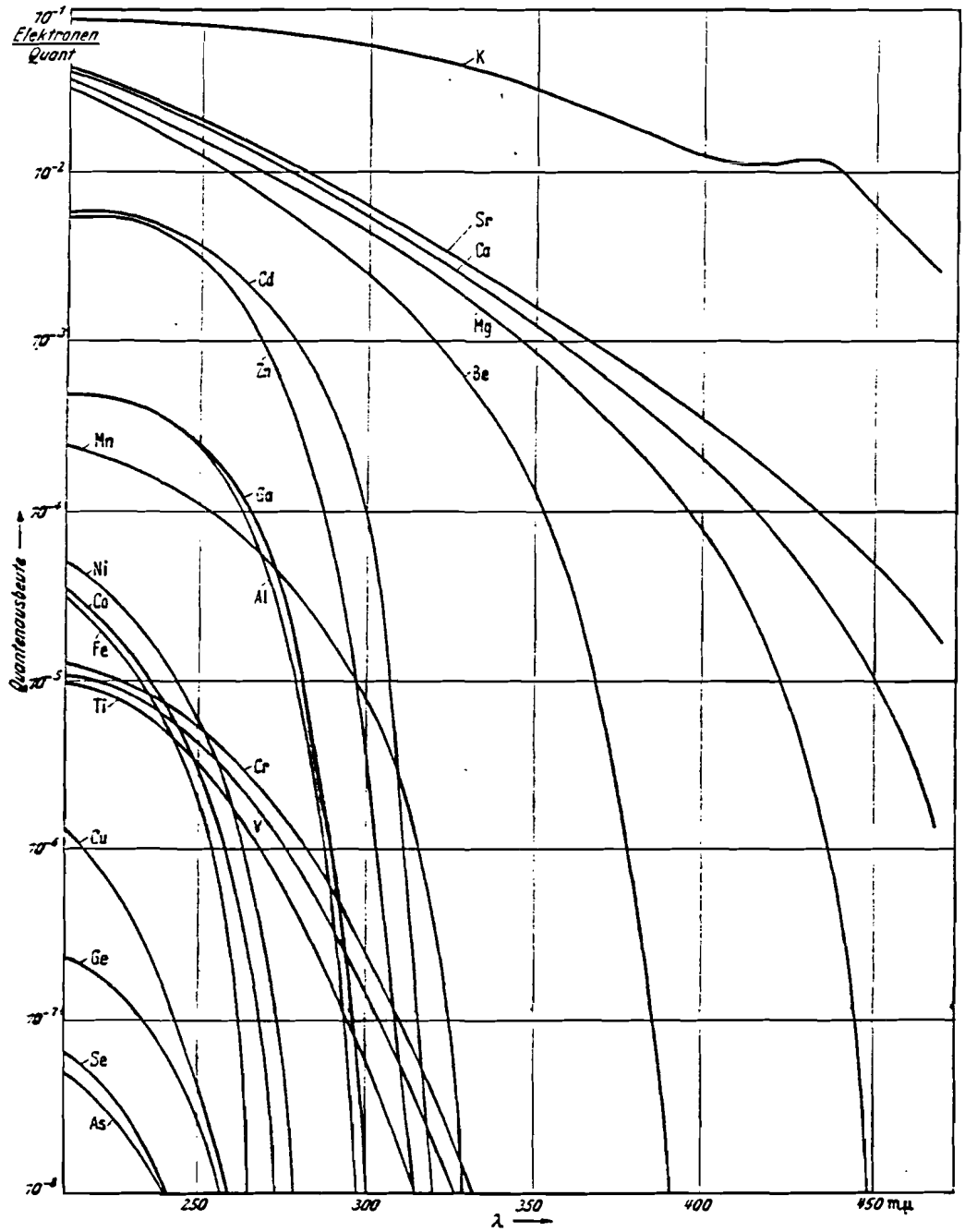

Fig. A2 Spectral photoelectric quantum efficiency of pure metals.

Fig. A3 shows quantum efficiency data for Ni and Cu for photon energies > 8 eV.

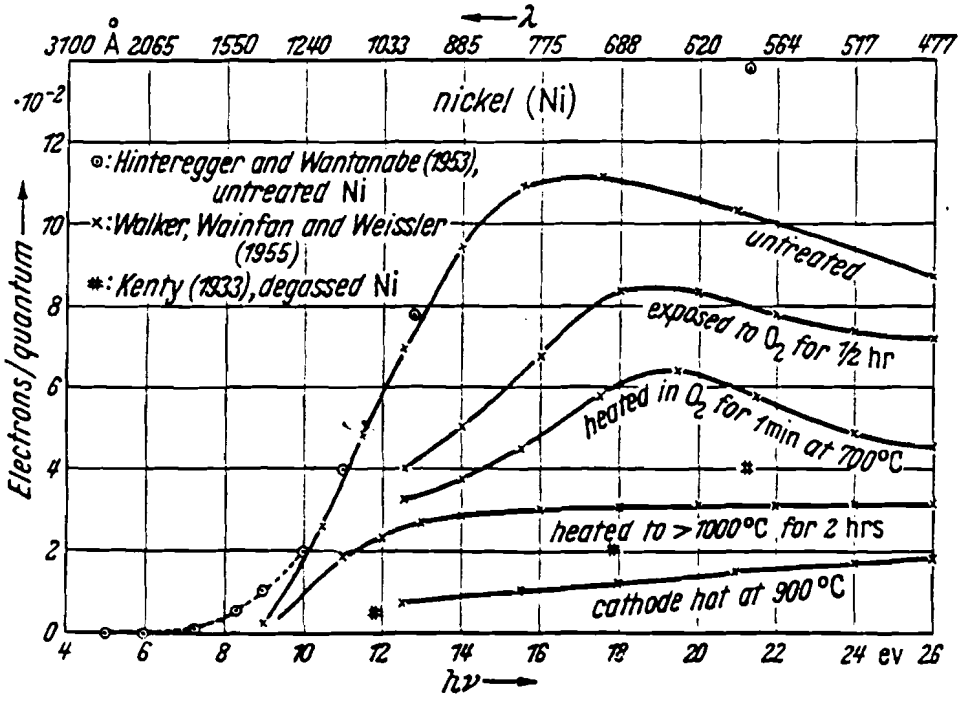

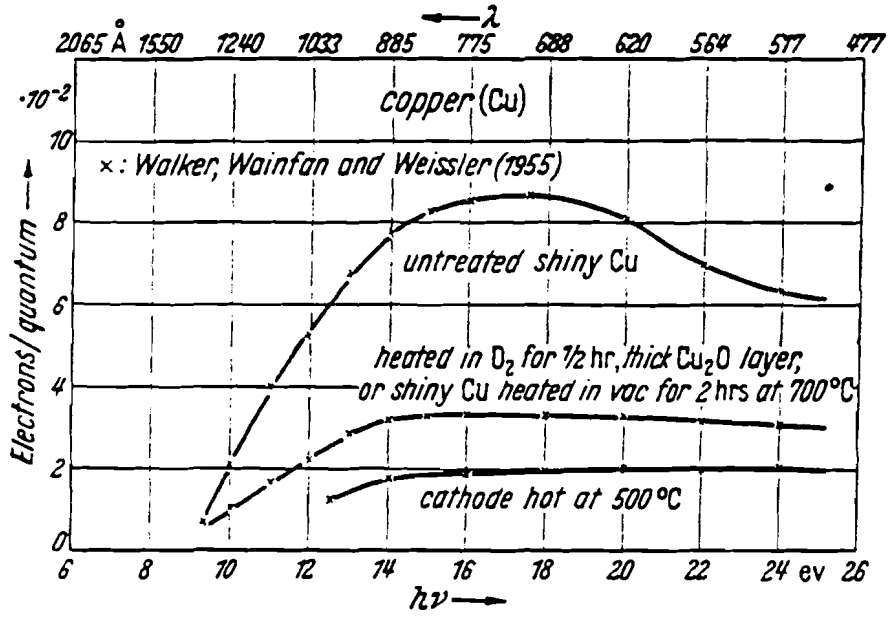

Fig. A3 Spectral yields for Ni and Cu for different surface treatments.